

Making methane visible

Magnus Gålfalk, Göran Olofsson, Patrick Crill, David Bastviken

Table of Contents

1. Supplementary Methods	2
2. Supplementary References	7
3. Supplementary Figures and Tables	8
Figure S1 - Illustration of hyperspectral imaging	8
Figure S2 - Model illustration of CH ₄ features	9
Figure S3 - Model illustration of CH ₄ , N ₂ O, and H ₂ O features	9
Figure S4 – Measured total sensitivity of the system	10
Figure S5 - Model uncertainties due to air humidity and temperature contrast	11
Figure S6 - CH ₄ mapping over an oligotrophic boreal lake	12
Figure S7 - High resolution spectra over an oligotrophic boreal lake	13
Table S1 - Comparison with recent remote sensing approaches yielding pixel based data	14

Supplementary Methods

Our method uses a novel hyperspectral camera, HyperCam Methane, that was custom-made for us by Telops (Canada) based on their HyperCam-LW (31). It has been optimized for CH₄ detection using a special detector with a built-in narrow band cold filter optimized for the strong thermal IR CH₄ band at 7.7 μm. Interference of light gives a spectrum for each pixel on the detector (320 x 256 pixels), producing a 25 x 20 degrees field of view with a 0.25x demagnifying telescope (6.25 x 5 degrees with our optional lens). The pixel field of view can thereby be selected to 0.34 or 1.36 mrad, producing spatial resolutions well below 1 m in both these modes (3.4/13.6 cm at 100 m and 17/68 cm at 500 m).

The natural abundance of CH₄ is ~1.8 ppmv, requiring high sensitivity for successful remote sensing and quantification over short distances at the landscape level, making the selected band suitable for sensitive CH₄ mapping from the ground or low altitudes. Most sensors at these wavelengths are sensitive to the full range 7.6 - 14.5 μm (the atmospheric N band). The strong CH₄ band at 7.7 μm (7.25-8.20 μm, peaking at 7.65 μm) is right at the lower wavelength end of most sensors. The sensors we are aware of have a large drop-off in sensitivity and only detect part of the band thus reducing the sensitivity for CH₄. In the 7.9-14.5 μm range, as far as CH₄ is concerned, any detector is only collecting photon noise from the thermal radiation of objects in a scene, decreasing the sensitivity. Thus, a great improvement in sensitivity for CH₄ detection can be made by using such a cold filter built into the detector. This also allowed exposure times of ~1.5 ms to be used, increasing the signal-to-noise ratio (S/N) substantially. As water vapor efficiently absorbs radiation (shaded areas in Supplementary Fig. 3) above ~1335 cm⁻¹ (below 7.49 μm) hiding any other lines, and with no strong CH₄ lines below 1260 cm⁻¹ (above 7.94 μm), we focused on the intermediate spectral region for modeling and quantification.

In addition to the high sensitivity of the system, the method has two additional important advantages: a high spectral resolution and the ability to map air motion during measurements. The spectral resolution of the system can be set as high as 0.25 cm⁻¹, clearly showing many individual CH₄ and H₂O spectral features, making fitting with spectral models very reliable because spectral regions can be selected where CH₄ lines are strong in between strong and sometimes saturated H₂O features (illustrated by e.g. Supplementary Fig 7). This avoids

mixing of CH₄ and stronger (possibly saturated) water lines which would otherwise degrade the S/N.

The modeling of the data is based on spectroscopic and scene analysis. We have made spectroscopic models based on the HITRAN high-resolution spectroscopic database (32) of line parameters as input for our line by line radiative transfer model (LBLRTM), building a database of transmittance spectra for our spectral resolutions (often 0.25 or 1 cm⁻¹) for H₂O, CH₄ and N₂O for 1024 column densities. We then model each scene using gas layers (different temperatures of gas in e.g. released gas and foreground gas) with a background surface that includes sky reflection. The optimization using a database, fitting in selected spectral regions optimized for strong CH₄ and many H₂O features, respectively, and iterating towards a solution, allows for fast solutions even though all the combinations of column densities in the database are considered, with an interpolation as a last step in between the best-fit column density grid points. A fit can be made for each pixel in a scene (up to 320 x 256) producing a CH₄ image. The models calculate background, gas and air temperatures as well as take into account reflected cold sky radiation. Due to the high spectral resolution there is also a possibility to model air temperature variations along each line of sight by combining H₂O features with different absorption.

For each scene we have used an optical rangefinder (Newcon LRM 2200SI) targeted at a number of distance calibration points with uniform backgrounds, which when combined with modeled pixels of the same background targets give the average air humidity (in the form grams H₂O per meter) in a scene at the time of measurements. For each pixel the background distance can then be calculated without the rangefinder using only the total amount of H₂O found from the models.

Once the average CH₄ content has been mapped from spectra over the whole imaging period (based on the many individual interference images collected at high rate; several hundred images per second), gas and air motions during the same period can be followed at high temporal resolution by following gas features in individual images over time. This is possible because an imaging Fourier transform spectrometer takes thousands of IR interference images which are used to build the spectra (yielding one spectrum for each pixel). These images, which can be corrected to remove the interference, contain the full spectral region with many

H₂O and CH₄ lines. Flow variability and dispersion can therefore also be monitored by tracking movements of CH₄ (if the flux is high enough) or water vapor structures in the images during the time of image collection (e.g. Supplementary Movie 2). Thus, CH₄ identification, quantification and fluxes can be calculated from the instrument data alone without any additional instruments. This is at present not possible from remote sensing measurements using airplanes or satellites as they produce snapshots of the CH₄ distribution at one point in time, having to rely on *in-situ* instruments such as weather stations on the ground or meteorological archives to estimate near-ground fluxes. Model parameters such as air and background temperatures are also calculated directly from the data for each pixel and used in the spectral and scene modeling.

Some key characteristics of the hyperspectral approach we present can be summarized as follows (see also Supplementary Table 1 for comparisons with other remote sensing techniques):

- The instrument has a cooled filter that blocks light outside a narrow band around 7.7 μm (the strong CH₄ lines), increasing sensitivity (removing photon noise from thermal radiation outside this rather narrow band).
- The wavelength range makes the camera optimized for shorter distances in the landscape ensuring that only near-ground CH₄ is measured.
- Therefore the technique measures CH₄ close to the ground avoiding potential atmospheric interferences in airplane and satellite measurements.
- It works for both point and diffuse sources.
- It is independent of day or night, and of reflected solar light and solar angles, as long as there are temperature contrasts of 1 °C or more.
- It can use high spectral resolution (0.25 cm^{-1}), resolving individual H₂O and CH₄ features, allowing detailed and robust models and fitting of CH₄ in spectral regions almost free from H₂O lines.
- The high imaging frame rate (several hundred images per second) can be used to reveal gas motion for flux calculations, and the variability in a CH₄ release with high temporal resolution.
- Air and background temperatures (with the possibility to calculate air temperature variations along each line of sight and background distances from H₂O lines) are calculated from the

spectrum of each pixel (each pixel being 3.4x3.4 cm or 14x14 cm at 100 m distance, depending on the telescope used, illustrating the high spatial resolutions available).

- Everything needed for the spectral modeling, scene modeling, spectroscopy, average column densities, air motion, flow movies, and flux calculations are simultaneous as they are all calculated from the same set of data using a single instrument (e.g. no weather station or meteorological database required to estimate air motion for flux calculations, which is needed in many other methods, e.g. Tratt et al. (20)).

The sensitivity of this method for visualizing CH₄ depends on a number of factors related to the detector (e.g. possible pixel-to-pixel variations, detector temperature and quality), the routines used for the spectroscopic modeling and fitting (e.g. number of pixels used per CH₄ column modeled), background distance extraction, emissivities of background materials, air humidity, sky conditions (cold clear sky or cloudy), background homogeneity, spectral resolution, and most importantly the temperature contrast between the background and CH₄. Many of these factors are however often similar between scenes, leaving the temperature contrast as the main factor, with an accuracy that increases with temperature contrast (Supplementary Fig. 4). The second most important factor is the number of pixels averaged for each column density measurement. Note that we have only used a single pixel for each CH₄ measurement in all our five example scenes and that the sensitivity can be improved substantially in scenes when needed. Supplementary Fig. 4 shows measurements of how the total uncertainty (over 50 meters) varies with temperature contrast and pixel averaging (using nearby pixels or repeated measurements). We find that CH₄ mapping can be made down to a temperature contrast of 1 °C, with a column density uncertainty of ~70, 25, 18, 12 ppmv·m for a single pixel, 8, 16, and 32 averaged pixels, respectively. At 100 m distance, 16 pixels correspond to a spatial resolution of 0.56 m² showing that highly sensitive measurements are possible with 1 m² resolution even with a temperature contrast of only 1 °C. The uncertainty decreases drastically to ~12, 8, 3, and 2 ppmv·m for $\Delta T = 10$ °C. This means detecting an increase of 0.01 ppmv extending 200 meters, or 2 ppmv in a 1 m thick gas cloud for 32 averaged pixels. We also find that it is common in natural and anthropogenic scenes to find temperature contrasts of at least 1 °C. Clear examples are sunlit leaves, grass, or rocks, where a 2-5 °C contrast is not uncommon. For anthropogenic scenes, such as gas from a chimney, the temperature difference is often even higher and CH₄ is seen in layers of both emission (anthropogenic source) and absorption (foreground air) further facilitating sensitive

quantification. Because distances are given by spectral modeling of H₂O lines and rangefinder distance calibration points, correcting for the foreground CH₄ is readily done. Supplementary Fig. 5 shows the calculated uncertainties of the spectroscopic modeling from humidity and temperature contrast (the two factors that would dominate the total uncertainty for a pure IR imaging system without spectroscopy). The uncertainty-contributions from these factors are typically low compared to the total uncertainty (Supplementary Fig. 4) and are mainly related to the determination of the background temperature.

Natural emissions of CH₄ are characterized by a mix of (a) high emissions during short time periods (e.g. bubbling from sediments occurring a few seconds followed by long quiet periods) or spatially constrained areas (e.g. flux through emergent aquatic vegetation in nutrient rich wetlands, or zones with natural seepage of geothermal CH₄), and (b) low but continuous fluxes over large areas (e.g. diffusive CH₄ emissions across lake surfaces). This leads to a high spatiotemporal variability in the natural fluxes that we hitherto do not understand completely because we have lacked methods to visualize all these flux types over extended areas at high enough spatial resolution. The low but continuous natural fluxes are most challenging to visualize and measure spectroscopically. We here provide an example showing that our system is sensitive enough to quantify CH₄ gradients over an oligotrophic boreal lake, Lilljön, near Norrköping, Sweden, a lake that had the lowest CH₄ emissions of all boreal lakes in a previous global review (previously measured fluxes from Lillsjön were 0.4-1.2 mg CH₄ m⁻² d⁻¹) (28; 29), and such nutrient poor boreal forest lakes are in general emitting less CH₄ per m² than temperate and tropical lakes (30). Using trees and hills, heated by the sun, as background we mapped CH₄ in the air above this lake during 11.2 minutes using 14 cubes (48 s cube⁻¹) and a spectral resolution of 0.25 cm⁻¹. The wind speeds were low (average 0.6 m s⁻¹) and the temperature contrasts varied in the range of 1 - 15 °C depending on the material and geometry of the background surfaces. The resulting column density map (Supplementary Fig. 6a) shows that small differences in CH₄ content along different lines of sight are readily detected, as trees at slightly different distances are seen through different amounts of ambient CH₄. After calculating a background distance map, a distant-independent CH₄ map can be calculated (Supplementary Fig. 6b) highlighting regions with excess CH₄ emission. In Supplementary Fig. 7 we present example spectra in the two lines of sight indicated in Supplementary Fig. 6a, with the corresponding model best fits over-plotted. The spectral resolution is high enough to clearly separate the CH₄ peak and the nearby H₂O line,

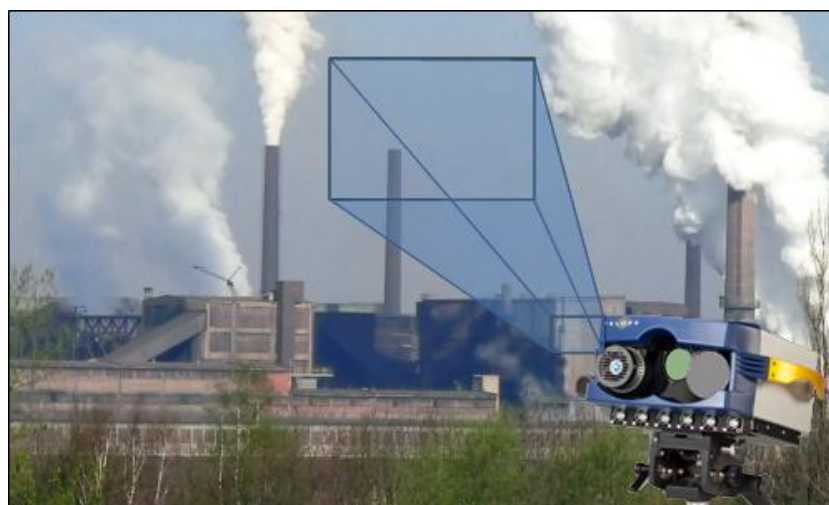
improving the sensitivity of the modeling and making graphical validation of the fit more reliable. *In situ* point measurements at the shore using the LGR gave CH₄ mixing ratios varying in the range 1.80-1.95, which is in agreement with the mixing ratios calculated in the camera CH₄ map (1.8-2.0; Supplementary Fig. 6b). The ability of our system to quantify such weak concentration gradients opens new opportunities to identify and map distributions of also natural CH₄ sources with low emissions per m².

Supplemental References

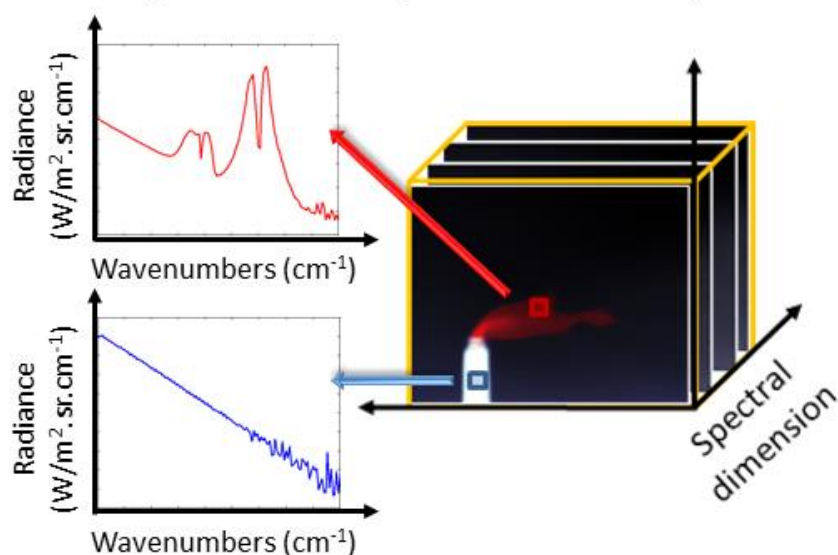
(see main article for references 1-27)

28. Bastviken, D. *et al.* Methane emissions from lakes: Dependence of lake characteristics, two regional assessments, and a global estimate. *Global Biogeochem. Cycles* **18**, GB4009 (2004). doi:10.1029/2004GB002238.
29. Schilder, J. *et al.* Spatial heterogeneity and lake morphology affect diffusive greenhouse gas emission estimates of lakes. *Geophysical Research Letters* **40**, 5752-5756 (2013).
30. Bastviken, D. *et al.* Freshwater Methane Emissions Offset the Continental Carbon Sink. *Science* **331**, 50 (2011).
31. Farley, V. *et al.* Performance of the FIRST, a Longwave Infrared Hyperspectral Imaging Sensor. *Proc. SPIE* 6398, 63980T (2006).
32. Rothman, L. S. *et al.* The HITRAN 2008 molecular spectroscopic database. *Journal of Quantitative Spectroscopy & Radiative Transfer* **110**, 533-572 (2009).

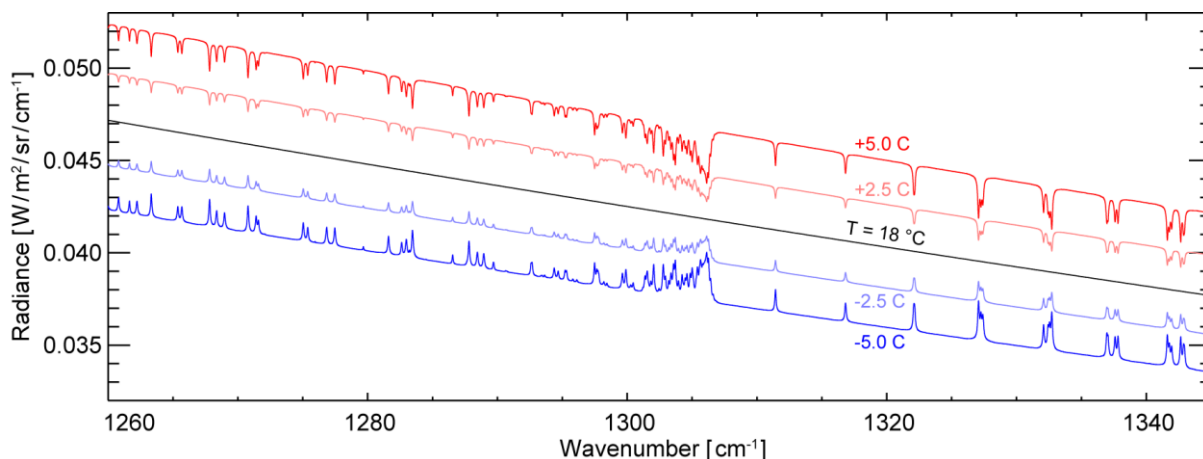
Supplementary Figures and Tables



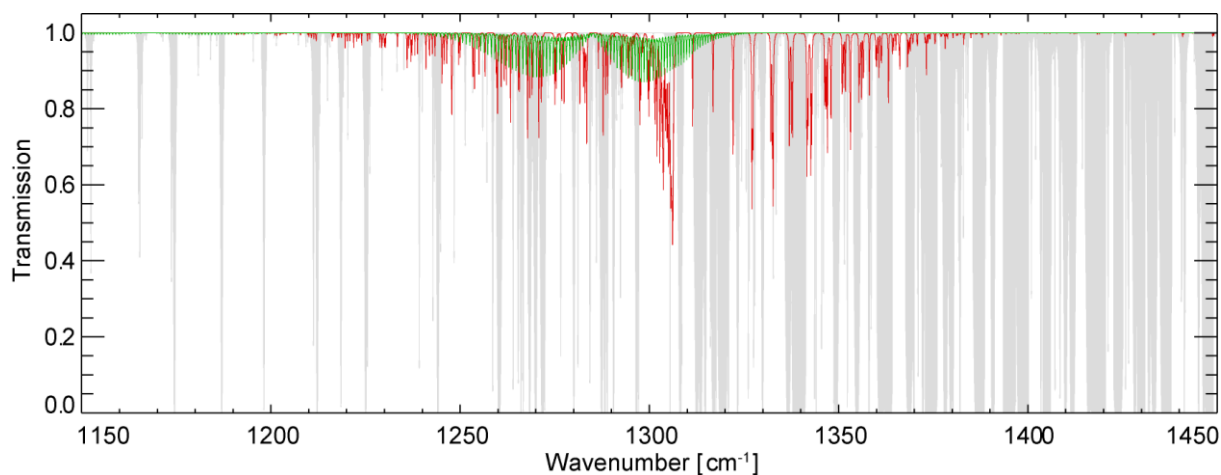
A high resolution spectrum for each pixel



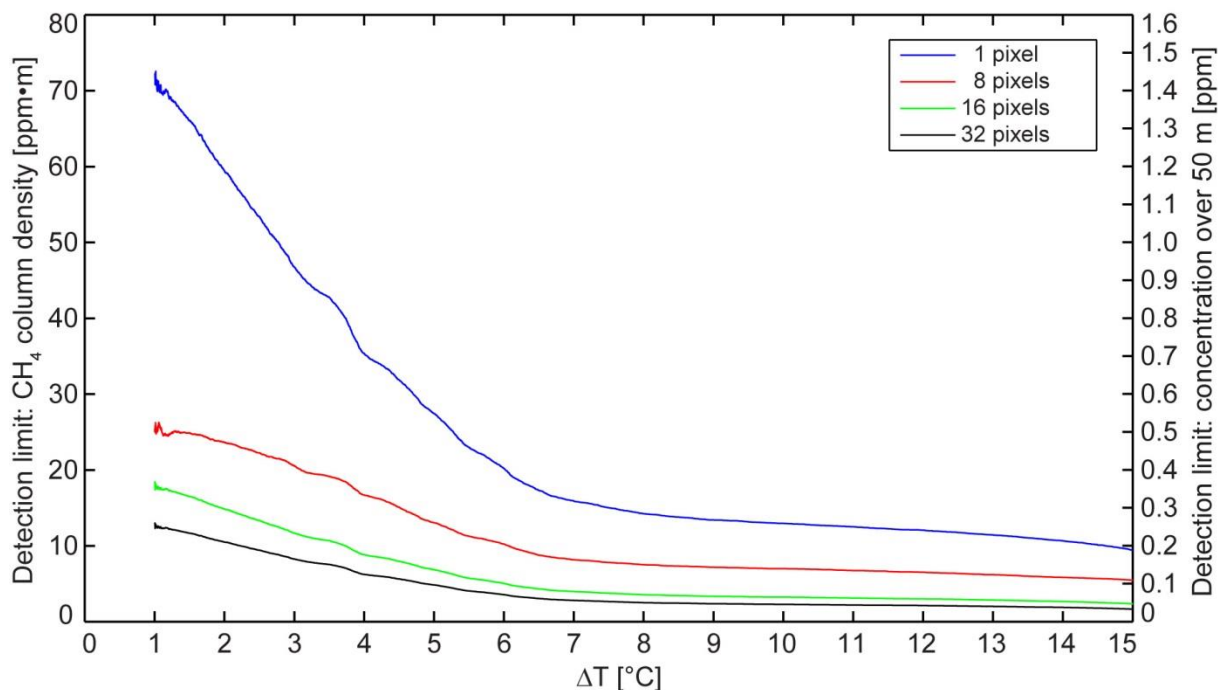
Supplementary Figure 1. Illustration of hyperspectral imaging - a spectrum is obtained for each pixel in a scene using imaging Fourier Transform Spectroscopy. This way data are stored in a cube with two spatial and one spectral dimension. By modeling each spectrum the total amount of CH₄ gas along each line of sight (column densities) can be calculated. This illustration was provided by and used with the permission of Telops Inc., Canada.



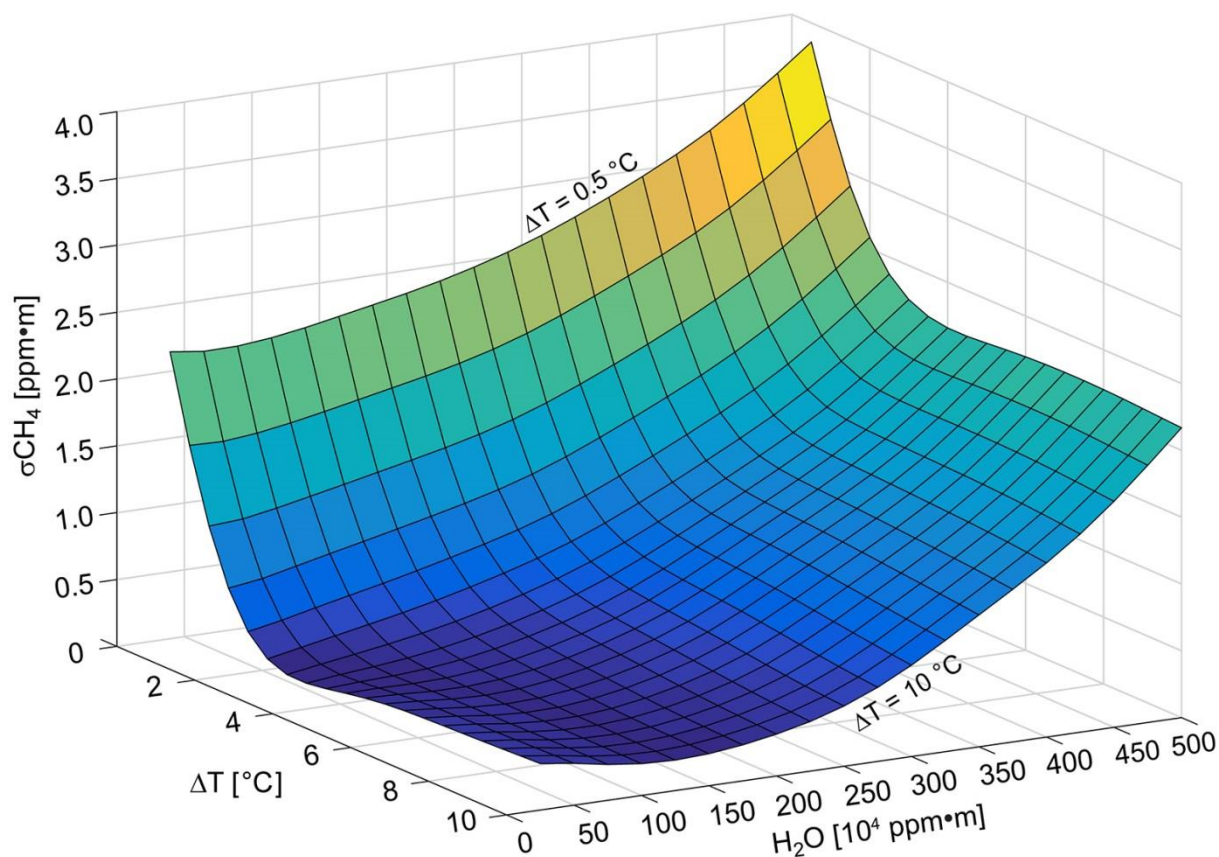
Supplementary Figure 2. Model illustration of CH₄ features for four different background – air temperature differences (air temperature 18 °C, CH₄ at ambient ~1.8 ppmv level, background distance 150 m). For warmer or colder backgrounds than the air, this CH₄ signature shows up as absorption or emission lines, respectively.



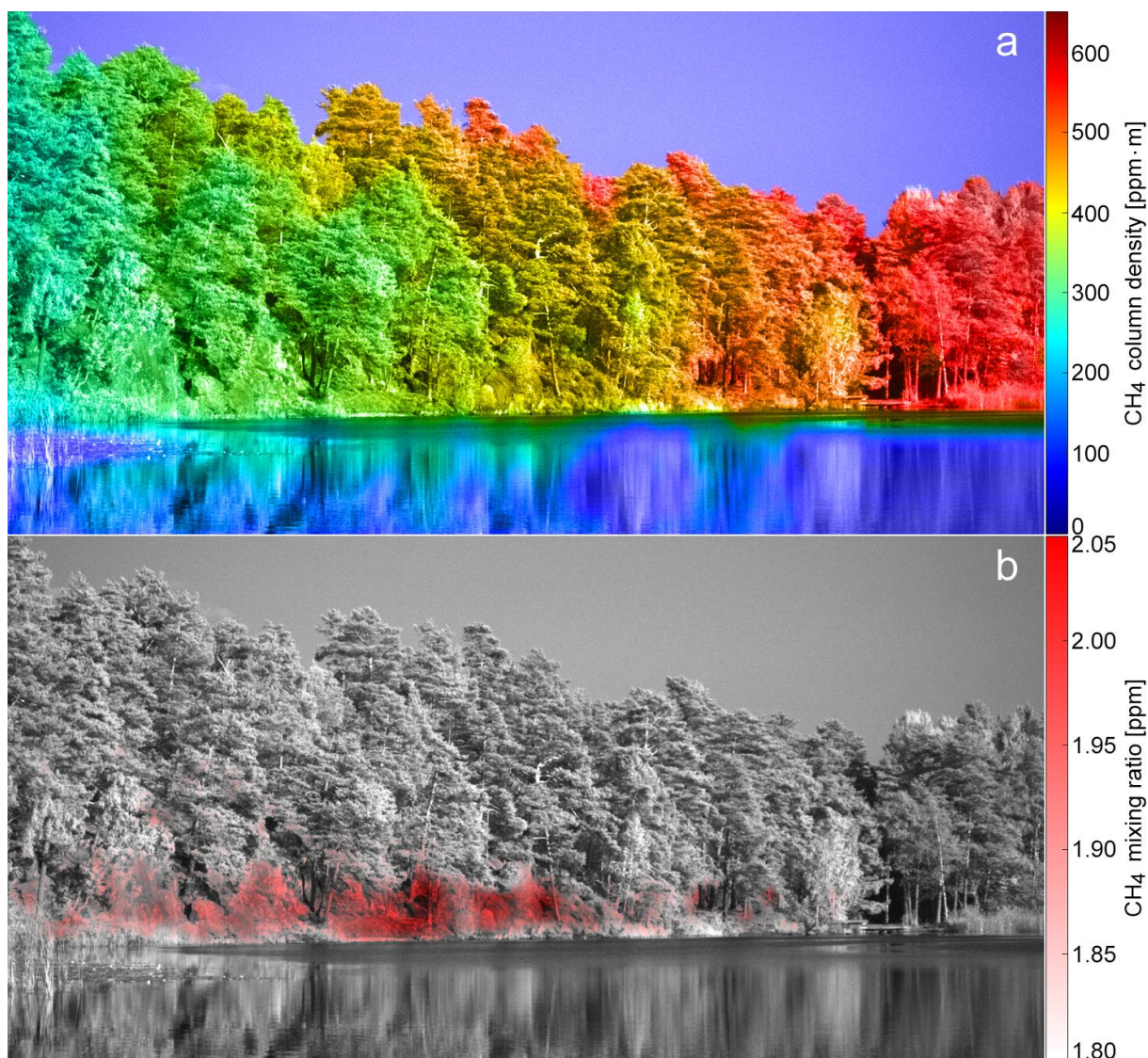
Supplementary Figure 3. Model illustration of CH₄ (red), N₂O (green) and H₂O (shaded) features. Model parameters are trace gases at ambient concentrations (CH₄ 1.8 ppmv, N₂O 0.32 ppmv, and H₂O at saturation level for 18 °C) and a background distance of 150 meters. All these species were included and separated in the spectral modelling.



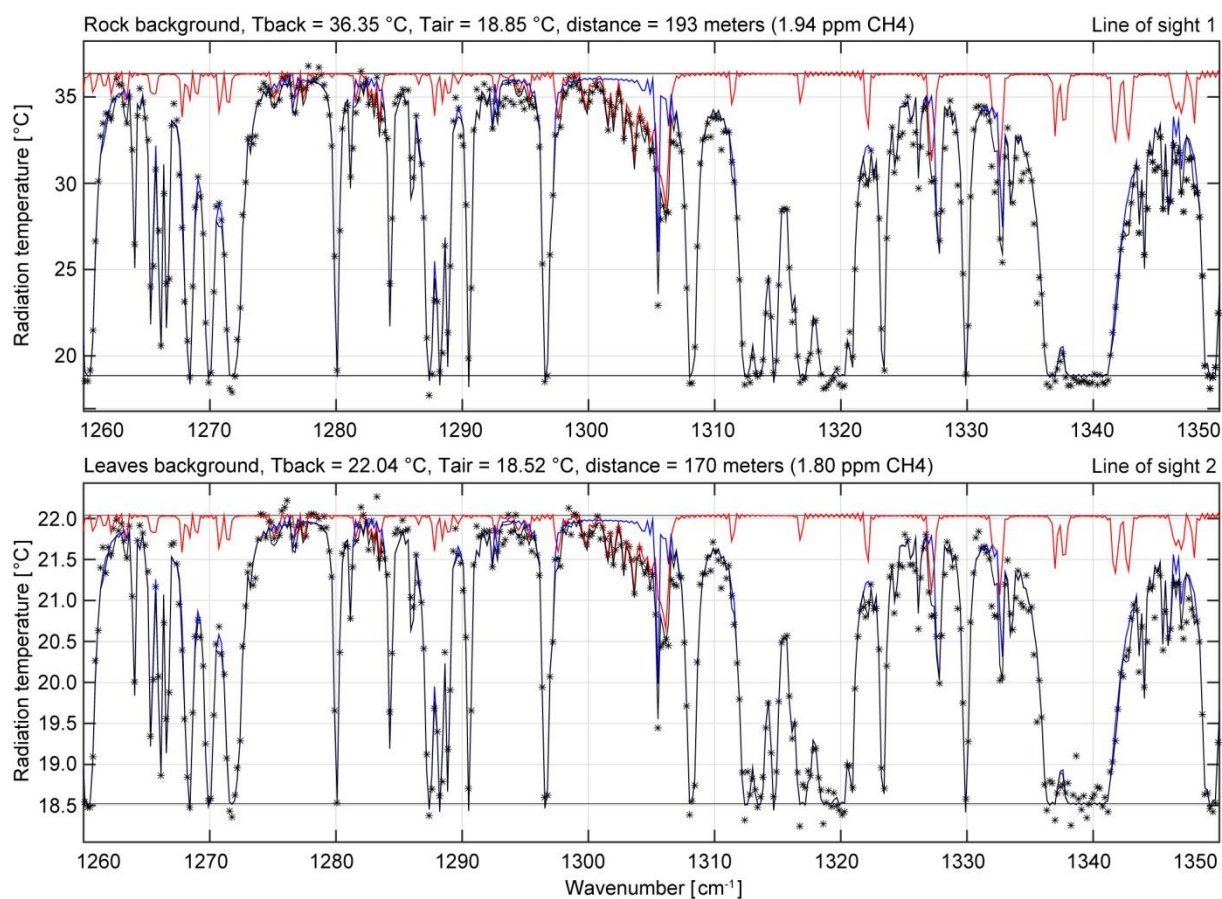
Supplementary Figure 4. Sensitivity of the system, calculated from measured scenes with a background distance of 50 meters and an ambient CH_4 mixing ratio of ~ 1.8 ppmv. The curves indicate how the sensitivity changes with background – gas temperature contrast ΔT for different averaging of spectra (using adjacent pixels or repeated measurements). Sensitivity is here given both as a distance independent detection limit (left axis) valid up to several hundred meters, and exemplified as a detection limit in average concentration over 50 meters (right axis). Note that typical detection limits for groups of >8 pixels (<0.5 ppm over 50 m) is well below background CH_4 levels (1.8 ppm) opening possibilities to identify CH_4 sink areas with levels below the atmospheric background (see also Supplementary Methods below).



Supplementary Figure 5. Uncertainties in the spectroscopic modeling due to air humidity and temperature contrast ($\Delta T = T_{\text{back}} - T_{\text{air}}$). Air humidity is plotted as H_2O column density in units of 10^4 ppm·m which is equivalent to distance in meters for ambient air with a relative humidity close to 100% at 18 °C. Plotted ranges are 0.5-10.0 °C (in steps of 0.5 °C) and 25-500 ppm·m (in steps of 25 ppm·m). Note that the uncertainty, ranging from 0.2 to 4 ppm·m never exceed the sensitivity shown in Supplementary Fig. 4.



Supplementary Figure 6. Mapping and quantification of the CH₄ gradient above the nutrient poor lake Lillsjön, having the lowest CH₄ emissions among the boreal lakes studied in (28) (14 cubes, acquisition time 11.2 min). The calculated column density map (**a**) shows the total amount of CH₄ along all lines of sight in the image. Background distances range from 120 to 350 meters (resulting in increasing amounts of CH₄ per lines of sight from left to right due to increasing background distance) with a field of view of 25 x 9.4°. After division with distances, a map of mixing ratios shows areas with excess CH₄ (**b**). The squares marked with numbers in panel **a** mark the locations of the two selected spectra shown in Supplementary Fig. 7. See also text regarding this figure in Supplementary Methods.



Supplementary Figure 7. Measured spectra at 0.25 cm^{-1} spectral resolution for the two example lines of sights in Supplementary Fig. 6a. The red, blue and black curves represent fitted model spectra of CH₄, H₂O, and their total absorption. Measurement points are plotted using small asterisks as symbols. See also text regarding this figure in Supplementary Methods.

Supplementary Table 1. Comparison with recent remote sensing approaches yielding pixel based data.

Property	This approach	Mako (20)	AVIRIS (18; 19)	GOSAT satellite (7)
Targeted wavelength region	Thermal IR (7.7 μm)	Thermal IR (7.7 μm)	SWIR (2.3 μm)	SWIR (1.6 μm)
Spectral resolution (cm^{-1})	0.25	7.4	20	0.27
Spatial elements simultaneously	320 x 256	1 x (400 – 2750)	1 x 640	1 (circle)
Typical operational distances (m)	20 – 750	~1000 m	4000 – 20 000	Entire atm.
Angular field of view (deg)	25 x 20	0.032 x 84 (one scan line)	0.057 x 34 (one scan line)	0.905 diam.
Field of view at operational range of distances	8.7 m x 7 m 327 m x 262 m	1 km x scan length	1.2 – 11 km x scan length	10.5 km diam. every 160 km
Spatial resolution range for operational distances to background (m)	0.03 - 1	1 – 2	4 - 20	10.5 km diam.
Temporal measurements per acquisition	6 000 – 10 000 per cube	1 per overpass	1 per overpass	76 336 per cube
Minimum reported column density (ppm·m)	10 (one pixel) 2 (16 pixels)	440	360	Not measured (only mixing ratio)
Minimum reported CH ₄ flux (g h^{-1})	25	2200	Not possible yet	---
Additional sources needed to estimate fluxes	None	Wind sensor close to CH ₄ source	Wind sensor close to CH ₄ source	Inverse models
Map air/CH ₄ motion from spectral data?	Yes	No	No	No
Target background	Any with temp. contrast	Any with temp. contrast	In the direction of Solar glint	In the direction of Solar glint